

Figure 1: A height map with cliff-like discontinuities (a), its color-coded gradient map (b), as could be obtained by photometric stereo methods, and a binary mask (c) showing the location of the cliffs. Note that the gradient map is oblivious to the cliffs, and gives no clue as to which end of the ramp (if any) is at ground level.

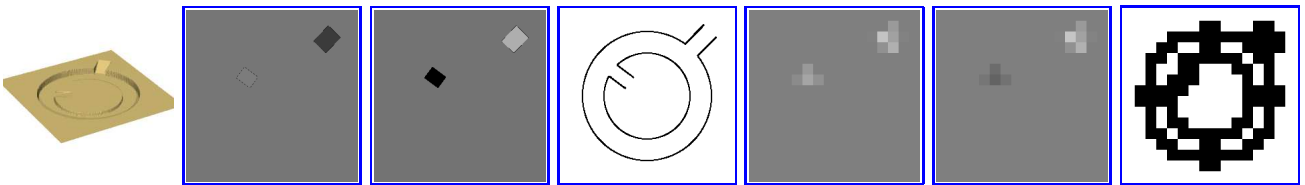


Figure 2: Example of region disconnection in grid-based multi-scale integration. From left to right: perspective view of a height map  $Z = Z(X, Y)$  with discontinuities, its derivatives  $F^{(0)} = \partial Z / \partial X$  and  $G^{(0)} = \partial Z / \partial Y$  sampled on a  $256 \times 256$  grid, a  $256 \times 256$  binary mask  $W^{(0)}$  showing the location of the height discontinuities in the domain (in black), and the maps  $F^{(4)}$ ,  $G^{(4)}$ , and  $W^{(4)}$  resulting from 4 steps of filtering and sub-sampling. Note that the central disk has become disconnected from the surrounding areas.

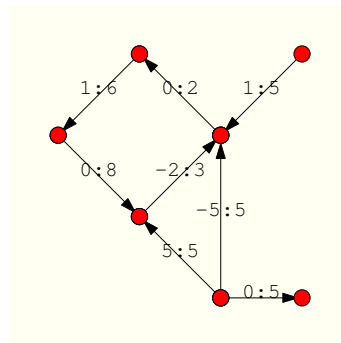


Figure 3: A small weighted differences mesh. The edge labels are the pairs  $d[e] : w[e]$ . Note that only one of the edges  $e, \text{SYM}(e)$  are illustrated.

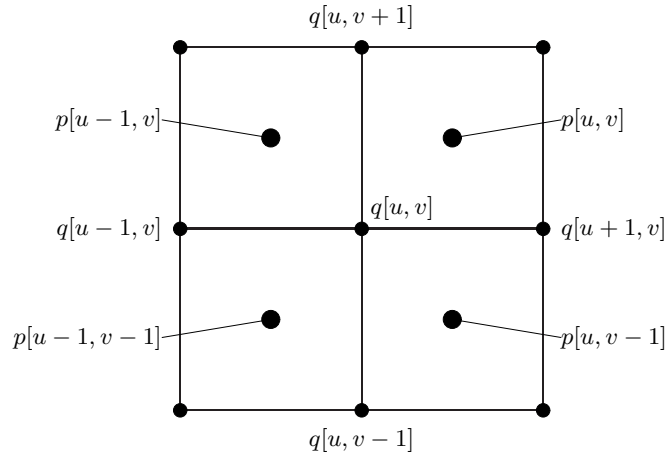


Figure 4: Gradient and  $Z$  sampling points adjacent to the point  $q[u, v] = (u, v)$ .

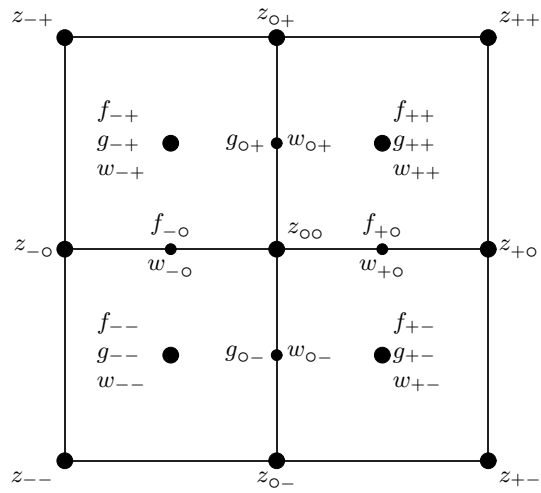


Figure 5: Notation for the interpolated  $Z$ , gradient and weight values around the point  $q[u, v]$ .

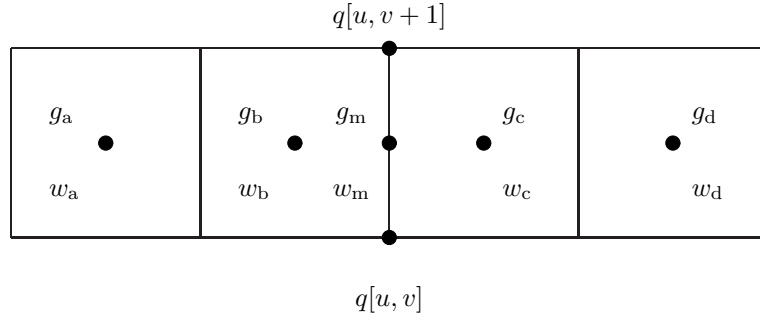


Figure 6: Interpolating the derivative  $\partial Z/\partial y$  in the point  $(u, v + \frac{1}{2})$ .

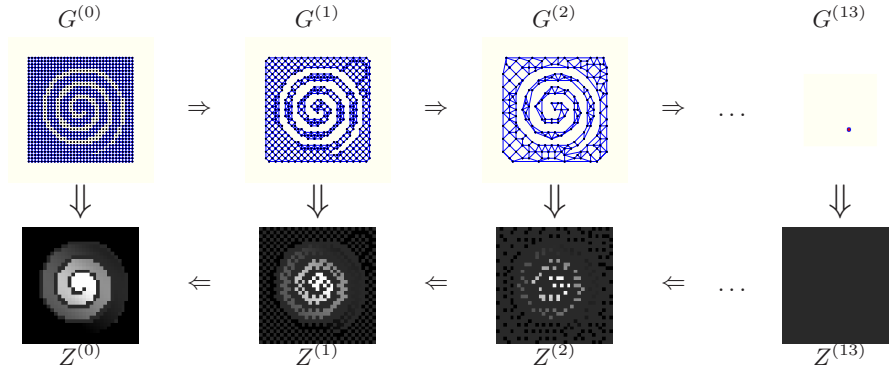


Figure 7: Multi-scale mesh integration.

---

Procedure  $\text{MSMESHINTEGRATE}(G, q, \varepsilon)$

1. If  $\#\mathcal{V}G = 1$  then
  2. Let  $v$  be the single vertex in  $\mathcal{V}G$ ; do  $z[v] \leftarrow 0$ ;
  3. else
  4.  $G' \leftarrow \text{DECIMATE}(G)$ ;
  5.  $\beta \leftarrow \#\mathcal{V}G' / \#\mathcal{V}G$ ;
  6.  $z' \leftarrow \text{MSMESHINTEGRATE}(G', q/\sqrt{\beta}, \varepsilon\sqrt{\beta}, )$ ;
  7.  $z \leftarrow \text{INTERPOLATE}(z', G)$ ;
  8.  $z \leftarrow \text{SOLVESYSTEM}(z, G, q, \varepsilon)$ ;
  9. Return  $z$ .
- 

Figure 8: Main procedure of the multi-scale integrator for weighted difference meshes

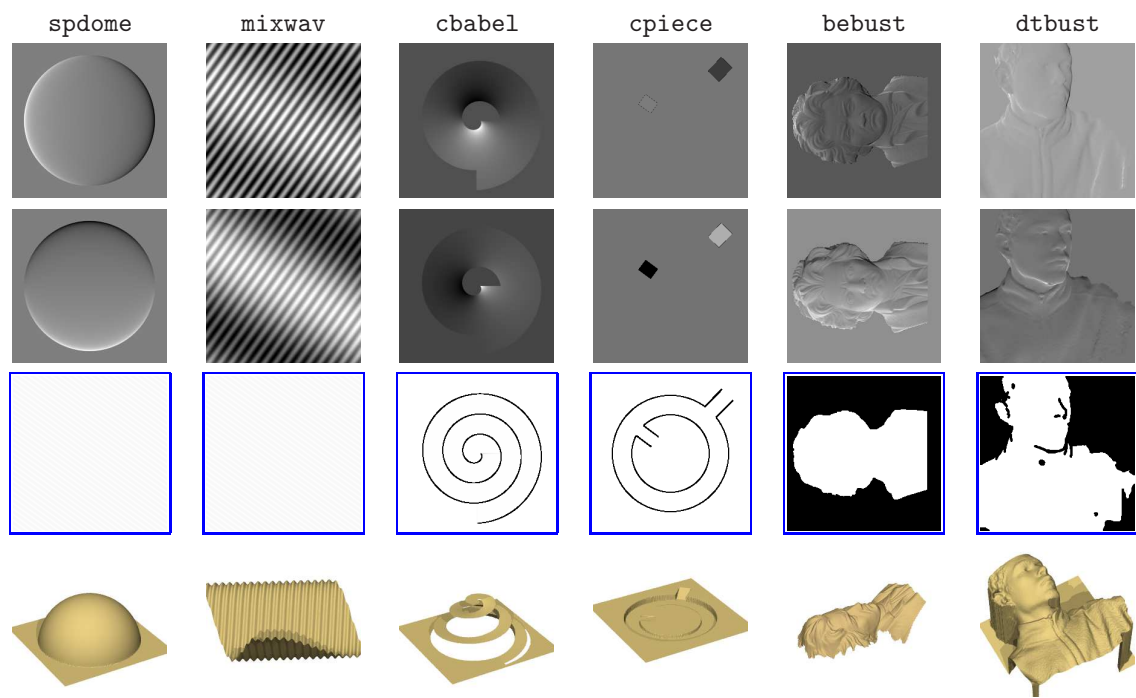


Figure 9: The test datasets, showing the gradient maps  $f$  (top row) and  $g$  (second row), the weight maps  $w$  (third row), and the correct  $z$  height map (bottom row).

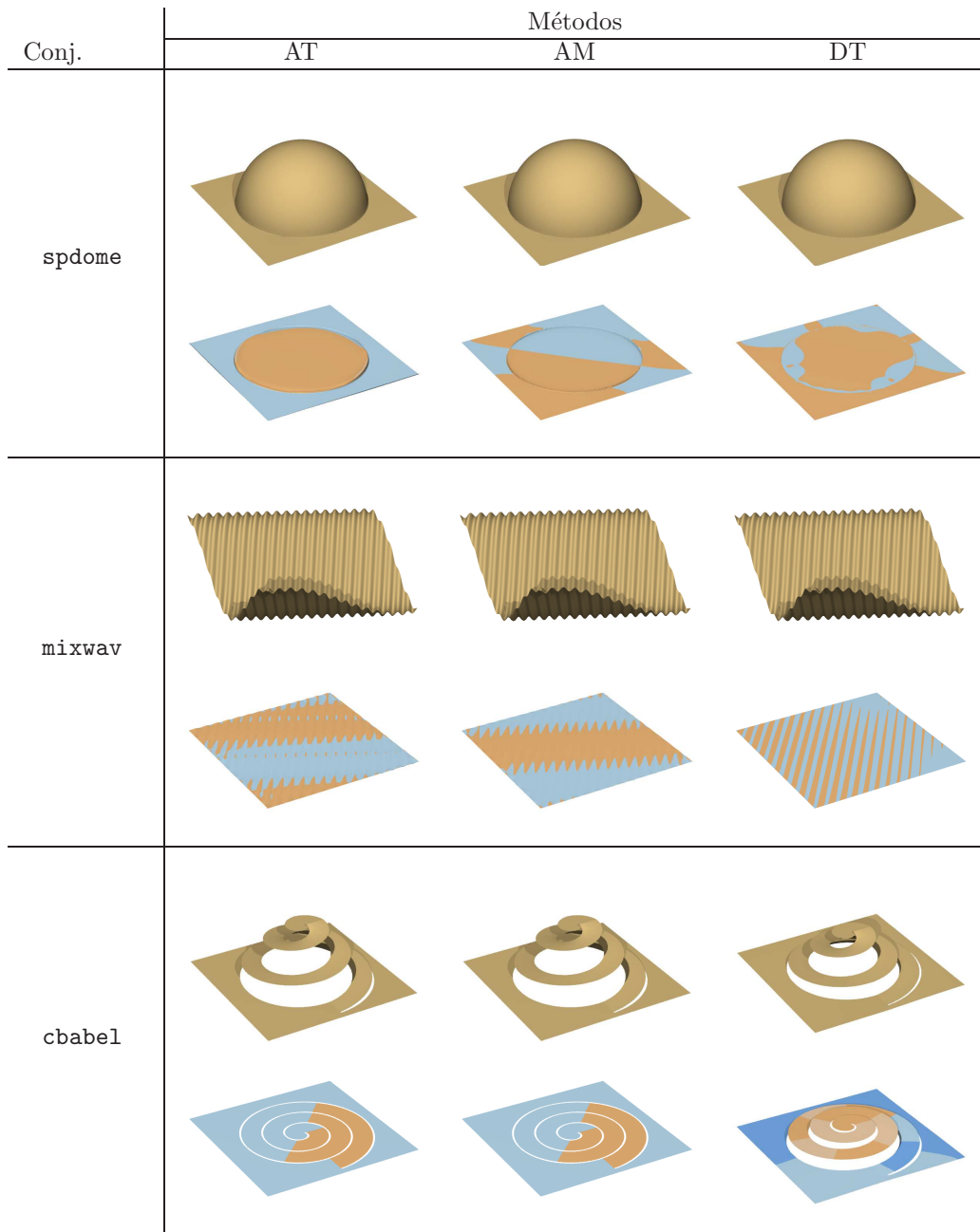


Figure 10: The height maps computed by algorithms AT, AM, and AT on the datasets `spdome`, `mixwav`, and `cbabel`, without noise. Blue and orange hues on the error maps show that the computed height was below or above the correct height, respectively.

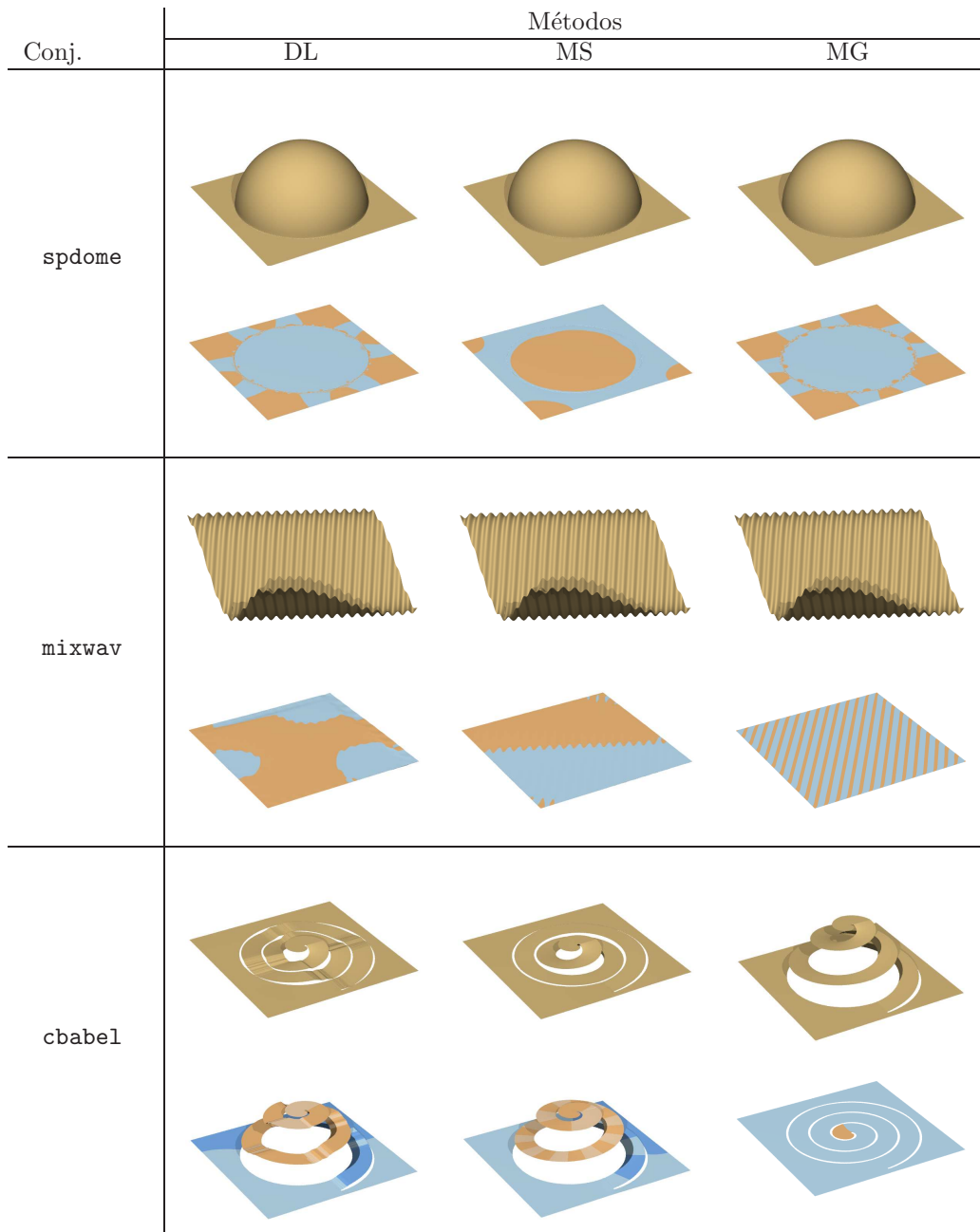


Figure 11: The height maps computed by algorithms DL, MS, and MG on the datasets `spdome`, `mixwav`, and `cbabel`, without noise .

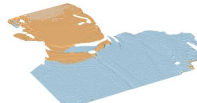
| Conj.  | Métodos   |   |   |
|--------|---|---|---|
|        | AT  | AM  | DT  |
| cpiece |    |   |    |
|        |    |   |    |
| bebust |    |    |    |
|        |  |  |  |
| dtbust |  |  |  |
|        |  |  |  |

Figure 12: The height maps computed by algorithms AT, AM, and DT on the datasets cpiece, bebust, and dtbust, without noise .

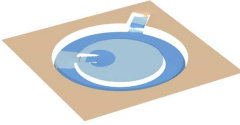
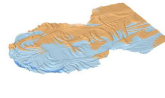
| Conj.  | Métodos   |   |   |
|--------|---|---|---|
|        | DL  | MS  | MG  |
| cpiece |    |   |    |
|        |    |   |    |
| bebust |    |    |    |
|        |  |  |  |
| dtbust |  |  |  |
|        |  |  |  |

Figure 13: The height maps computed by algorithms DL, MS, and MG on the datasets cpiece, bebust, and dtbust, without noise .

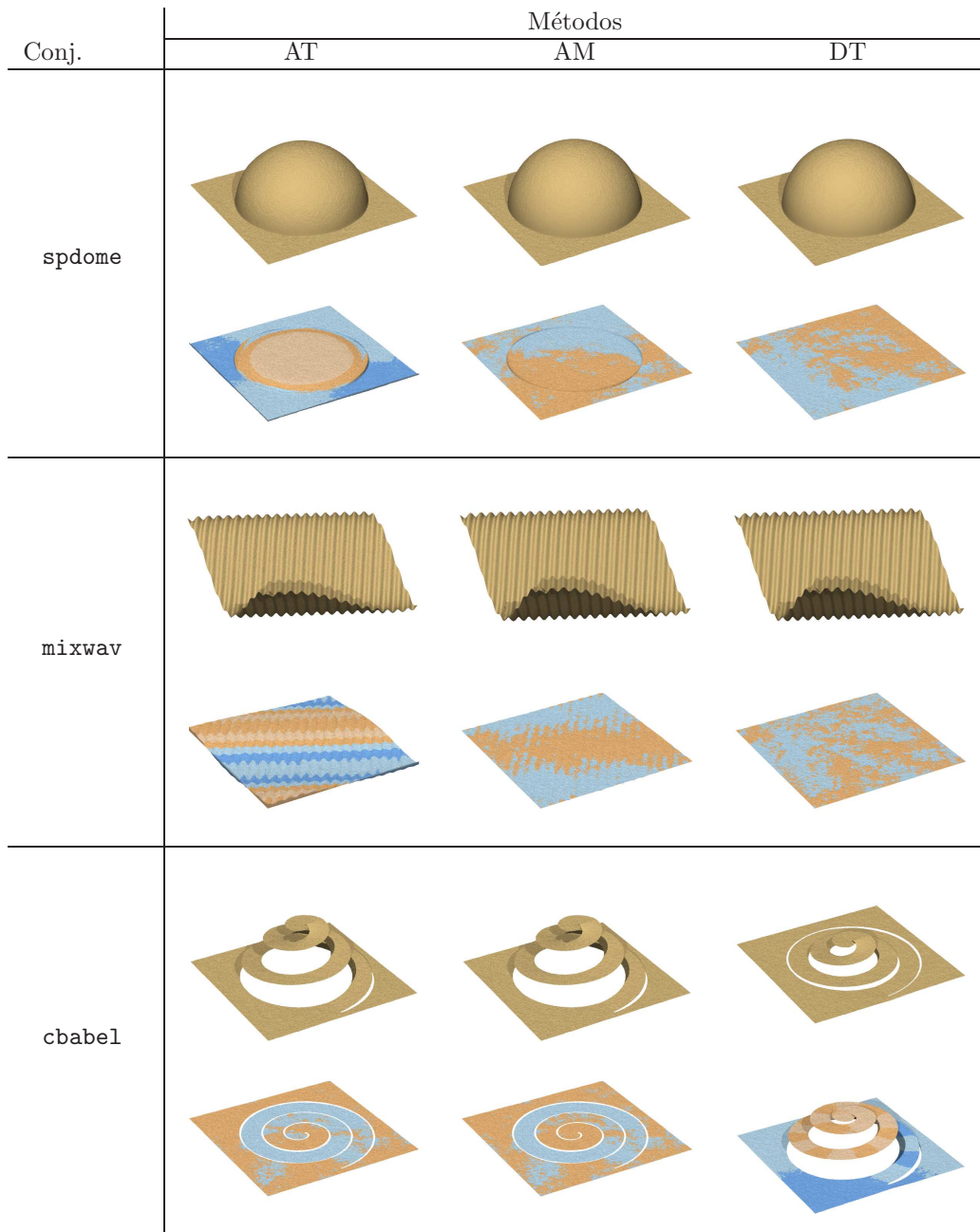


Figure 14: The height maps computed by algorithms AT, AM, and DT on the datasets `spdome`, `mixwav`, and `cbabel` with 30% of Gaussian noise.

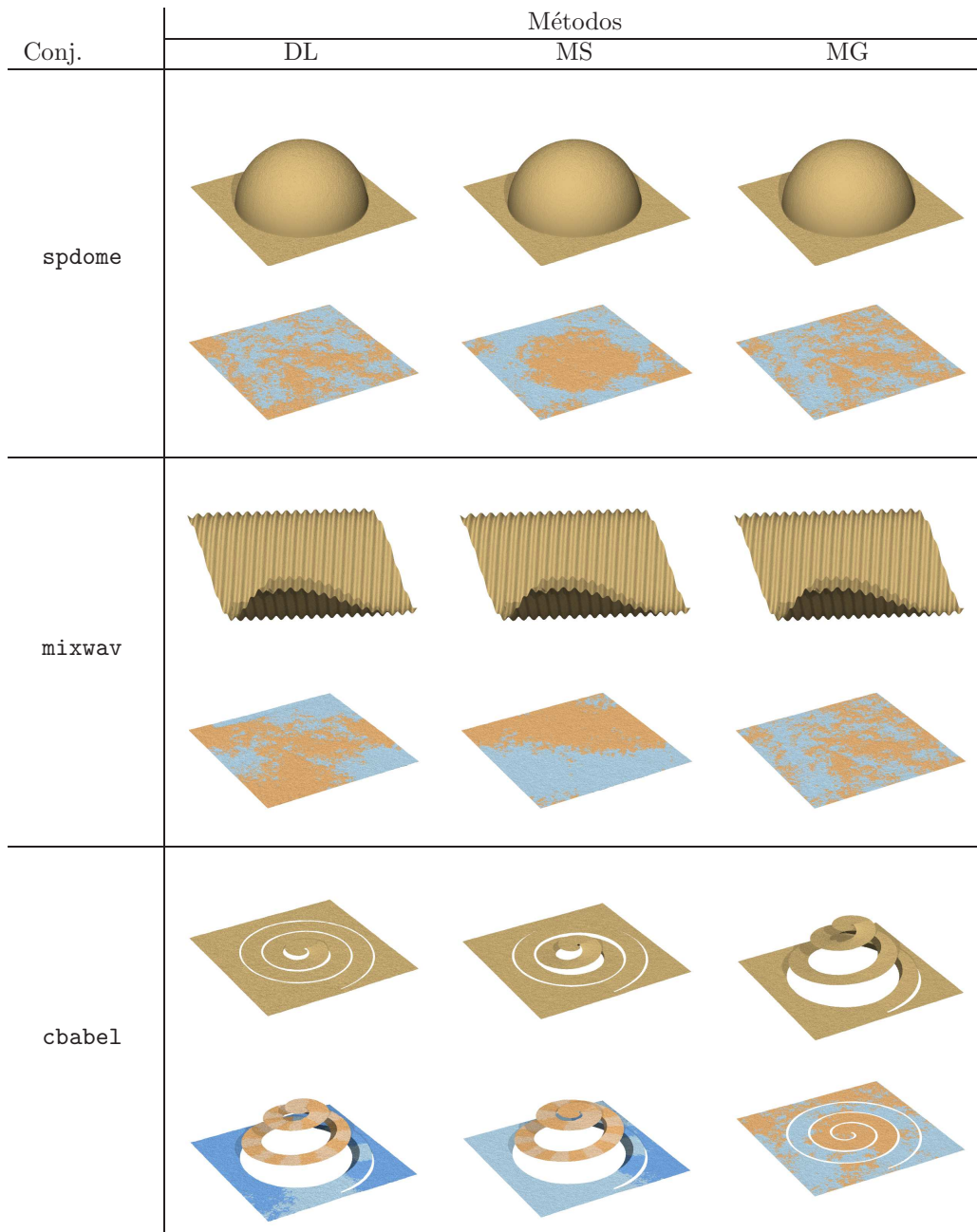


Figure 15: The height maps computed by algorithms DL, MS, and MG on the datasets `spdome`, `mixwav`, and `cbabel` with 30% of Gaussian noise.

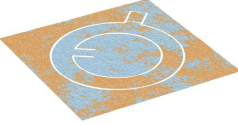
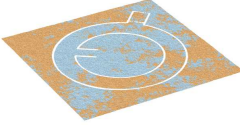
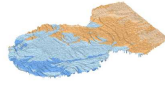
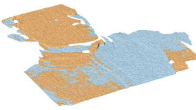
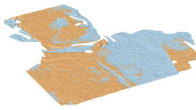
| Conj.  | Métodos   |   |   |
|--------|---|---|---|
|        | AT  | AM  | DT  |
| cpiece |    |   |    |
|        |    |   |    |
| bebust |    |    |    |
|        |  |  |  |
| dtbust |  |  |  |
|        |  |  |  |

Figure 16: The height maps computed by algorithms AT, AM, and DT on the datasets cpiece, bebust, and dtbust with 30% of Gaussian noise.

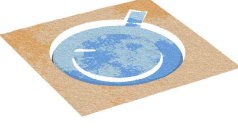
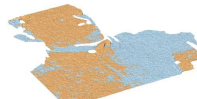
| Conj.  | Métodos   |   |   |
|--------|---|---|---|
|        | DL  | MS  | MG  |
| cpiece |    |   |    |
|        |    |   |    |
| bebust |    |    |    |
|        |  |  |  |
| dtbust |  |  |  |
|        |  |  |  |

Figure 17: The height maps computed by algorithms DL, MS, and MG on the datasets cpiece, bebust, and dtbust with 30% of Gaussian noise.

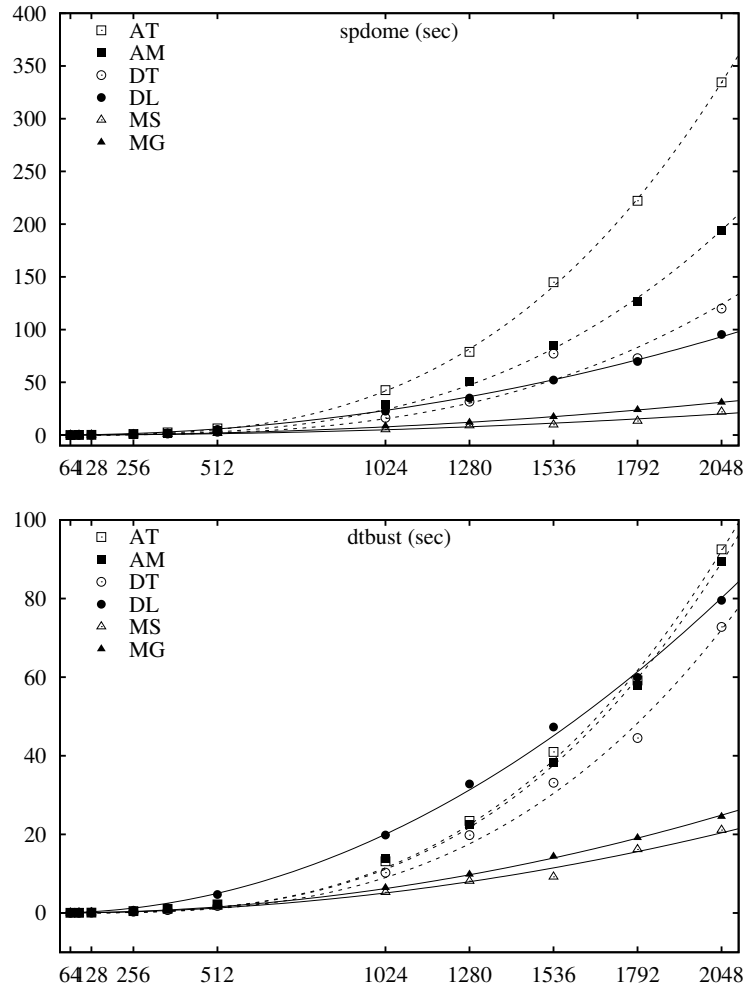


Figure 18: Plots of the system solving time for the four single-scale methods (AT, AM, DT, and DL), the uniform grid multi-scale method (MS) and the graph multiscale method of this article (MG), for the `spdome` and `dtbust` datasets. Note that the plots are in function of  $n = N^2$  in order to aid the visualization. The fitted curves are  $\alpha n^2 = \alpha N$  (full) and  $\alpha n^3 = \alpha N^{1.5}$  (dotted) with the best-fit coefficient  $\alpha$ .